Coupled finite element/boundary element approach for fluid–structure interaction

Gordon C. Everstine and Francis M. Henderson
Applied Mathematics Division, David Taylor Research Center, Bethesda, Maryland 20084

(Received 23 July 1989; accepted for publication 24 November 1989)

A new computational capability is described for calculating the sound-pressure field radiated or scattered by a harmonically excited, submerged, arbitrary, three-dimensional elastic structure. This approach, called NASHUA, couples a NASTRAN finite element model of the structure with a boundary element model of the surrounding fluid. The surface fluid pressures and normal velocities are first calculated by coupling the finite element model of the structure with a discretized form of the Helmholtz surface integral equation for the exterior fluid. After generation of the fluid matrices, most of the required matrix operations are performed using the general matrix manipulation package available in NASTRAN. Farfield radiated pressures are then calculated from the surface solution using the Helmholtz exterior integral equation. The overall capability is very general, highly automated, and requires no independent specification of the fluid mesh. An efficient, new, out-of-core block equation solver was written so that very large problems could be solved. The use of NASTRAN as the structural analyzer permits a variety of graphical displays of results, including computer animation of the dynamic response. The overall approach is illustrated and validated using known analytic solutions for submerged spherical shells subjected to both incident pressure and uniform and nonuniform applied mechanical loads.

PACS numbers: 43.20.Tb, 43.30.Jx

INTRODUCTION

Two fundamental problems in structural acoustics are (1) the calculation of the farfield acoustic pressure field radiated by a general, submerged, three-dimensional, elastic structure subjected to internal time-harmonic loads and (2) the calculation of the farfield acoustic pressure scattered by an elastic structure subjected to an incident time-harmonic wavetrain. These problems can be solved by combining a finite element model of the structure with a fluid loading computed using finite element,[1–3] boundary element,[4–14] combined finite element/analytical,[15,16] or T-matrix[17,18] techniques. In addition, a boundary element fluid model has also been combined with a boundary element structural model.[19] Chen[20] recently reviewed developments occurring in this area up to about 1982.

Although all these approaches are computationally intensive for large structural models, the most practical approach for accurate, large-scale, computational structural acoustics predictions is probably the coupled finite element/boundary element approach. The fluid finite element approach is burdened with the additional complications caused by the approximate radiation boundary condition at the outer fluid boundary, the requirements on mesh size and extent (sometimes leading to frequency-dependent fluid meshes[3]), and the difficulty of generating the fluid mesh.

In contrast, the boundary element or boundary integral equation (BIE) approach for generating the fluid loading is mathematically exact (except for surface discretization error) and requires little or no additional modeling effort to convert an existing model of a dry structure for use in submerged analyses. The boundary element approaches cited above differ from each other in geometric generality (three-dimensional or axisymmetric), structural formulation (direct or modal), fluid formulation (simple source or Helmholtz integral equation), order of fluid polynomial approximation (constant, linear, or quadratic), and method of avoiding the interior characteristic frequencies. In addition, the various approaches differ in such practical considerations as the finite element code used and the degree of automation in the implementation.

Here, we describe a new, large-scale computational capability known as NASHUA, which couples a NASTRAN[21,22] finite element model of a structure with a fluid loading calculated with a discretized form of the Helmholtz surface integral equation. None of the capabilities developed previously to solve the fluid–structure interaction problem was developed for a widely used structural analysis code such as NASTRAN.

This implementation differs from the previous approaches in several important ways. First, the use of NASTRAN allows considerable generality in the structural model, including the capability to treat internal fluid volumes.[23,24] In addition, the acoustic analysis of a structure can be integrated with other dynamic and stability analyses, and many of the pre- and postprocessors developed for use with NASTRAN (e.g., computer animations[25]) can be used. Moreover, the reduction in structural stiffness caused by hydrostatic pressure can be easily accounted for using the geometric stiffness matrix used in elastic stability analyses.[14]

Second, no independent fluid mesh need be specified.

The NASHUA approach locates fluid grid points at the wet structural points (rather than at structural element centroids) and obtains normals and areas by applying a unit, outwardly directed static pressure load on the wet surface. Since a first-order fluid approximation is used (to allow convenient coupling with the first-order shell elements often used by the finite element practitioners), explicit integration over the surface elements is avoided by using Chertock's approach[26] to compute the influence of a fluid point on itself (the "self" terms in the fluid matrices). This approach also avoids the more costly numerical evaluation of integrals used in other formulations.

Third, a new out-of-core block equation solver[27] was written to solve efficiently the large, complex, fully populated, nonsymmetric system of algebraic equations that arises. As a result, very large problems (with tens of thousands of structural degrees of freedom) can be solved.

In general, the finite element program (NASTRAN) is used to generate the structure's stiffness, mass, and damping matrices and to perform various matrix manipulations. Other programs are used to generate the fluid matrices, perform the field calculations, and display the results.

The purposes of this paper are to describe the theoretical approach used and to demonstrate its validity by comparing calculated results with closed-form or classical series solutions for acoustic radiation and scattering from spherical shells. For the radiation calculations, both uniformly driven and sector-driven shells will be considered.

I. THEORETICAL APPROACH

A. The structure

Consider an arbitrary, submerged, three-dimensional, elastic structure subjected to either internal time-harmonic loads or an external time-harmonic incident pressure wavetrain. If the structure is modeled with finite elements, the resulting matrix equation of motion for the structural degrees of freedom (DOF) can be written as

$$Zv = F - GAp, \tag{1}$$

where Z is the structural impedance matrix (dimension $s \times s$), v is the complex amplitude of the velocity vector for all structural DOF (wet and dry) in terms of the coordinate systems selected by the user ($s \times r$), F is the complex amplitude of the vector of mechanical forces applied to the structure ($s \times r$), G is the rectangular transformation matrix of direction cosines to transform a vector of outward normal forces at the wet points to a vector of forces at all points in the coordinate systems selected by the user ($s \times f$), A is the diagonal area matrix for the wet surface ($f \times f$), and p is the complex amplitude of total fluid pressures (incident + scattered) applied at the wet grid points ($f \times r$). In this equation, the time dependence $\exp(i\omega t)$ has been suppressed, where $i = (-1)^{1/2}$, and ω is the circular frequency of excitation. In the above dimensions, s denotes the total number of independent structural DOF (wet and dry), f denotes the number of fluid DOF (the number of wet points), and r denotes the number of load cases. If first-order finite elements are used for the surface discretization of the structure, surface areas, normals, and the transformation matrix G can be obtained from the calculation of the load vector resulting from an outwardly directed static unit pressure load on the structure's wet surface.

In Eq. (1), the structural impedance matrix Z, the matrix that converts velocity to force, is given by

$$Z = (-\omega^2 M + i\omega B + K)/i\omega, \tag{2}$$

where M, B, and K are the structural mass, viscous damping, and stiffness matrices, respectively. For structures with a nonzero loss factor, K is complex.

B. The exterior fluid

The total fluid pressure p satisfies the Helmholtz differential equation

$$\nabla^2 p + k^2 p = 0, \tag{3}$$

where $k = \omega/c$ is the acoustic wavenumber and c is the speed of sound in the fluid. Equivalently, for smooth surfaces, p is the solution of the Helmholtz integral equation[7,28]

$$\int_S p(\mathbf{x}) \frac{\partial D(r)}{\partial n} dS - \int_S q(\mathbf{x}) D(r) dS = \begin{cases} p(\mathbf{x}')/2 - p_I, & \mathbf{x}' \text{ on } S, \\ p(\mathbf{x}') - p_I, & \mathbf{x}' \text{ in } E, \\ -p_I, & \mathbf{x}' \text{ in } I, \end{cases} \tag{4}$$

where S, E, and I denote surface, exterior, and interior fluid points, respectively; p_I is the incident free-field pressure, r is the distance from $\mathbf{x}$ to $\mathbf{x}'$ (i.e., from P_j to P_i in Fig. 1), D is the Green's function

$$D(r) = e^{-ikr}/4\pi r, \tag{5}$$

$$q = \frac{\partial p}{\partial n} = -i\omega\rho v_n, \tag{6}$$

ρ is the mass density of the fluid, and v_n is the outward normal component of velocity on S. As shown in Fig. 1, $\mathbf{x}$ in Eq. (4) is the position vector for a typical point P_j on the surface S, $\mathbf{x}'$ is the position vector for the point P_i that may be either on the surface or in the exterior field E, the vector $\mathbf{r} = \mathbf{x}' - \mathbf{x}$, and $\mathbf{n}$ is the unit outward normal at P_j. We denote the lengths of the vectors $\mathbf{x}$, $\mathbf{x}'$, and $\mathbf{r}$ by x, x', and r, respectively. The normal derivative of the Green's function D appearing in Eq. (4) can be evaluated as

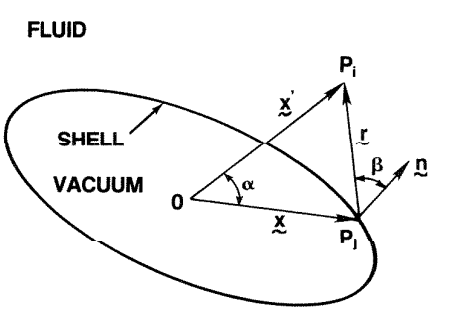

FIG. 1. Notation for the Helmholtz integral equation.

$$\frac{\partial D(r)}{\partial n} = \frac{e^{-ikr}}{4\pi r}\left(ik + \frac{1}{r}\right)\cos\beta, \tag{7}$$

where β is defined as the angle between the normal $\mathbf{n}$ and the vector $\mathbf{r}$, as shown in Fig. 1.

The substitution of Eqs. (5)–(7) into the surface equation (4) yields

$$\frac{p(\mathbf{x}')}{2} - \int_S p(\mathbf{x})\frac{e^{-ikr}}{4\pi r}\left(ik + \frac{1}{r}\right)\cos\beta\, dS = i\omega\rho \int_S v_n(\mathbf{x})\frac{e^{-ikr}}{4\pi r}dS + p_I, \tag{8}$$

where $\mathbf{x}'$ is on S. This integral equation relates the total pressure p and normal velocity v_n on S. If Eq. (8) is discretized for numerical computation, we obtain the matrix equation

$$Ep = Cv_n + p_I \tag{9}$$

on S. With first-order approximations to the integrals, E is evaluated as

$$E_{ij} = -(e^{-ikr}/4\pi r)(ik + 1/r)(\cos\beta_{ij})A_j, \quad r \neq 0, \tag{10}$$

where A_j is the area assigned to the point $\mathbf{x}_j$ and $r = r_{ij} = |\mathbf{x}_i - \mathbf{x}_j|$. Similarly,

$$C_{ij} = (i\omega\rho\, e^{-ikr}/4\pi r)A_j, \quad r \neq 0. \tag{11}$$

Surface areas are obtained from the finite element calculation of the load vector resulting from an outwardly directed static unit pressure load on the structure's wet surface. [The symbol "i" denotes the imaginary quantity $(-1)^{1/2}$ except when it is used in this section as a subscript.]

As was discussed by Wilton,[7] the use of first-order integration in Eqs. (10) and (11) yields the same order of accuracy as would be obtained if linear interpolation functions were used for the variation of pressure and velocity over the elements. This property is analogous to the situation in one-dimensional Newton–Cotes integration in which odd-point formulas are preferred to the next higher-order even-point formulas, since both have the same order of accuracy. Moreover, the integration scheme selected is particularly easy to implement since it requires a knowledge of only the normal and area assigned to each wet point rather than any information about the elements on the wet surface. However, as a result, the implementation is restricted to first-order finite elements (i.e., those without midsize nodes) on the wet surface.

These formulas for E_{ij} and C_{ij} are applicable only for the terms that do not involve the influence of a surface point on itself. For the self terms, for which $r = 0$, the integrals in Eq. (8) must be evaluated by a different approach. Consider first the velocity integral in Eq. (8). If we use Chertock's approach[26] and assume that v_n is constant over a small circular patch of radius b_i centered at $\mathbf{x}$, then, from Eq. (8),

$$C_{ii} = i\omega\rho \int_0^{2\pi}\int_0^{b_i} \frac{e^{-ikr}}{4\pi r} r\, dr\, d\theta, \tag{12}$$

where b_i is selected so that $\pi b_i^2 = A_i$, the total area assigned to the point. The evaluation of this integral yields

$$C_{ii} = i\omega\rho A_i/2\pi b_i, \tag{13}$$

where

$$b_i = (A_i/\pi)^{1/2}. \tag{14}$$

The evaluation of the self term E_{ii} is similar except that the curvature of the radiating surface must be taken into account because the singularity in the pressure term of Eq. (8) is one order higher than that of the velocity term.[26] Here, we assume that p is constant over a small spherical cap located at $\mathbf{x}_i$ and having curvature c_i and area A_i. Then, from Eq. (8),

$$E_{ii} = \frac{1}{2} - \int_0^{2\pi}\int_0^{b_i} \frac{e^{-ikr}}{4\pi r}\left(ik + \frac{1}{r}\right)\left(-\frac{rc_i}{2}\right) r\, dr\, d\theta, \tag{15}$$

where we have used the approximation

$$\cos\beta \simeq -rc_i/2. \tag{16}$$

The evaluation of this integral yields

$$E_{ii} = 1/2 + (1 + ikb_i)(c_iA_i)/(4\pi b_i), \tag{17}$$

where, for general structures, we interpret c_i as the mean curvature at $\mathbf{x}_i$.

The use of b_i in Eqs. (13) and (17) facilitates the calculation of the self terms at points lying in planes of symmetry, since A_i is divided by 2, 4, or 8 at such points, but b_i is computed from Eq. (14) as if the full area at the point were applicable.

The need to know the mean curvatures at each wet point is the major impediment to full automation of this procedure, since no mechanism has been (or could easily be) built into NASTRAN that enables the user to extract the curvature of a surface at a point. We handle this problem by placing some minor restrictions on the analyst so that the curvatures can be computed for the commonly occurring geometries of spheres, cylinders, conical sections, and flat sections. For other shapes, the curvatures must be supplied by the analyst.

In contrast to the situation for curvatures, the approach used for surface areas and normals is fully automated, since the user defines the wet surface by applying a static, outwardly directed, unit pressure load to that surface.

These discretizations of the Helmholtz surface integral equation yield fluid matrices E and C that are fully populated, complex, nonsymmetric, frequency-dependent matrices of dimension $f \times f$. In addition, the matrices E and C are singular at the discrete frequencies of the resonances of the corresponding interior acoustic cavity with Dirichlet (zero pressure) boundary conditions.[29] The singularities at such frequencies (referred to as the "characteristic," "critical," or "forbidden" frequencies of the problem) can be avoided by using, for example, the Schenck[29] or Burton and Miller[30] approaches. Schenck makes use of the third (interior) Helmholtz integral equation to generate a few additional equations that can be imposed as constraints on the system. In our implementation, we use this approach except that, rather than impose the constraints using an overdetermined system as Schenck did, we follow Rizzo's suggestion and impose the constraints using Lagrange multipliers.[31,32] The resulting system therefore remains square, and standard equation solvers can be used. Without some type of avoidance of the characteristic frequency problem, only low-frequency acoustic radiation and scattering could be handled, since the fundamental interior resonance occurs between $ka = 2.4$ and $ka = \pi$ for prolate spheroidal shapes.[33]

C. The coupled system

The vector of normal velocities v_n in Eq. (9) is related to the vector of total structural velocities v by the same rectangular transformation matrix G:

$$v_n = G^T v, \tag{18}$$

where the superscript T denotes the matrix transpose. If velocities v and v_n are eliminated from Eqs. (1), (9), and (18), the resulting equation for the coupled fluid–structure system is

$$Hp = Q + p_I, \tag{19}$$

where

$$H = E + CG^T Z^{-1} GA \tag{20}$$

and

$$Q = CG^T Z^{-1} F. \tag{21}$$

The formulation of the coupled problem in this way appears to have been first derived by Henderson.[5] Since H and Q depend on geometry, material properties, and frequency, Eq. (19) can be solved to yield the total surface pressures p. Since the two right-hand-side terms in Eq. (19) correspond to mechanical and incident loadings, respectively, only one of the two terms would ordinarily be present for a given case. Since H exhibits the same characteristic frequencies as E and C,[11] avoidance procedures must be used for the coupled fluid–structure formulation.

The vector v of velocities at all structural DOF may then be recovered by solving Eq. (1) for v:

$$v = Z^{-1}F - Z^{-1}GAp. \tag{22}$$

Surface normal velocities v_n may be recovered by substituting this solution for v into Eq. (18).

D. The field solution

With the solution for the total pressures and velocities on the surface, the exterior Helmholtz integral equation, Eq. (4), can be integrated to obtain the radiated (or scattered) pressure at any desired location $\mathbf{x}'$ in the exterior field. We first substitute Eqs. (5)–(7) into the second part of Eq. (4) to obtain a form suitable for numerical integration:

$$p(\mathbf{x}') = \int_S \left[i\omega\rho v_n(\mathbf{x}) + \left(ik + \frac{1}{r}\right) p(\mathbf{x}) \cos\beta \right] \frac{e^{-ikr}}{4\pi r} dS, \tag{23}$$

where all symbols have the definitions used previously, and $\mathbf{x}'$ is in the exterior field. Thus, with the total pressure p and normal velocity v_n on the surface S, the radiated or scattered pressure at $\mathbf{x}'$ can be determined by numerical quadrature using Eq. (23).

In applications, however, the field pressures generally of interest are in the farfield, so we develop an asymptotic form of Eq. (23) for use instead of Eq. (23). In the farfield, $x' \to \infty$ implies

$$ik + 1/r \to ik \tag{24}$$

and

$$\cos\beta \to \mathbf{n} \cdot \mathbf{x}'/x', \tag{25}$$

and, from the application of the law of cosines,

$$r \to x' - x\cos\alpha, \tag{26}$$

where α is the angle between the vectors $\mathbf{x}$ and $\mathbf{x}'$ (Fig. 1). Hence, in the farfield,[5]

$$p(\mathbf{x}') = \left(\frac{ike^{-ikx'}}{4\pi x'}\right) \int_S [\rho c v_n(\mathbf{x}) + p(\mathbf{x}) \cos\beta] \times e^{ikx\cos\alpha} dS, \tag{27}$$

where the asymptotic form, Eq. (25), is used for $\cos\beta$.

With the surface and farfield solutions, a variety of other quantities of interest can be computed, including average and root-mean-square surface velocities and pressures, surface acoustic intensity, radiated power, and radiation efficiency.[34] For example, the acoustic intensity at a point on the surface is the product of the pressure there and the component of normal velocity that is in phase with the pressure:

$$I = \mathrm{Re}(pv_n^*), \tag{28}$$

where the asterisk denotes the complex conjugate. (There is no factor 1/2 in this equation if we assume that pressures and velocities are already "effective" values rather than amplitudes. With this assumption, consistency is maintained, and there is no mixing of effective and peak quantities.) The total power radiated is the surface integral of acoustic intensity. Since, for low frequencies, the pressure p and the normal velocity v_n have nearly orthogonal phase (i.e., the fluid behaves like an added mass), the intensity calculation (and hence the power integral) can be sensitive to small errors in p and v_n on the surface. To circumvent this numerical problem, the radiated power can alternatively be computed by integrating the acoustic intensity over the farfield sphere, where pressure and velocity are in phase (since $p = \rho c v_n$). The calculation of farfield pressure is not sensitive to small errors in the surface solution, since it is calculated using the asymptotic form of the exterior Helmholtz integral equation, Eq. (27), which has the effect of smoothing out small errors in the surface solution.

E. Summary of the theoretical approach

The solution procedure uses the finite element program (NASTRAN) to generate the matrices K, M, B, and F and to generate sufficient geometry information so that the matrices E, C, G, A, and p_I can be computed by a separate program. Then, given all matrices on the right-hand sides of Eqs. (20) and (21), standard matrix operations are used to compute H and Q. Equation (19) is then solved for the total pressures p using Schroeder's block solver OCSOLVE.[27] Next, the surface normal velocities v_n and the vector v of velocities at all structural DOF are recovered to complete the surface and structural solutions. This calculation of H, Q, p, v_n, and v is repeated for each excitation frequency and the results merged. Then, with the total pressures and velocities on the surface, the asymptotic (farfield) form of the Helmholtz exterior integral equation is integrated to compute the farfield radiated pressures.

II. NUMERICAL EXAMPLES

In this section, three problems with known analytic (including series) solutions are solved to demonstrate the validity of the entire solution procedure.

A. Radiation from a uniformly driven spherical shell

Consider first the problem of the uniformly driven, submerged, spherical shell, a problem with a closed-form solution. In this problem, a thin-walled spherical shell is submerged in a liquid and driven internally with a spherically symmetric, time-harmonic pressure load. Since the solution is also spherically symmetric, the field solution depends only on radial distance from the origin.

We first derive the closed-form solution. The shell stiffness (the total static force required to increase the radius a unit amount) is

$$k_s = 8\pi Eh/(1-\nu), \tag{29}$$

where E and ν are the Young's modulus and Poisson's ratio for the shell material, and h is the thickness of the shell. The shell mass is

$$m_s = 4\pi a^2 h\rho_s, \tag{30}$$

where a is the mean shell radius and ρ_s is the density of the shell material. Hence, for a uniform time-harmonic pressure drive, the structural impedance for an undamped spherical shell is

$$Z_s = (\omega^2 m_s - k_s)i/\omega, \tag{31}$$

where ω is the circular frequency of the excitation.

For the surrounding fluid, the ratio of surface pressure to surface velocity is[29]

$$p/v = i\omega\rho a/(1+ika), \tag{32}$$

where ρ is the density of the fluid and $k=\omega/c$. Hence, the fluid impedance (ratio of total force to velocity) is

$$Z_f = i\omega\rho 4\pi a^3/(1+ika). \tag{33}$$

For the harmonically driven submerged shell, the surface velocity is therefore

$$v = 4\pi a^2 p_0/(Z_s+Z_f), \tag{34}$$

where p_0 is the amplitude of the internal pressure drive. Given the surface velocity v, the surface pressure can be recovered from Eq. (32). The fluid pressure in the exterior field decays with distance[35]; hence,

$$p_r = p(a/r)e^{-ik(r-a)}, \tag{35}$$

where p_r is the pressure at distance r from the origin and p is the pressure on the surface. Note that if the expression for surface velocity v obtained from Eq. (32) is substituted into the farfield radiated pressure formula, Eq. (27), Eq. (35) is obtained. [This property is necessary for the validation of the asymptotic formula, Eq. (27).]

We numerically solved the problem with the following characteristics[36]:

$a = 5$ m	shell radius
$h = 0.15$ m	shell thickness
$E = 2.07\times 10^{11}$ Pa	Young's modulus
$\nu = 0.3$	Poisson's ratio
$\rho_s = 7669$ kg/m^3	shell density
$\eta = 0$	shell loss factor
$\rho = 1000$ kg/m^3	fluid density
$c = 1524$ m/s	fluid speed of sound
$p_0 = 1$ Pa	internal pressure

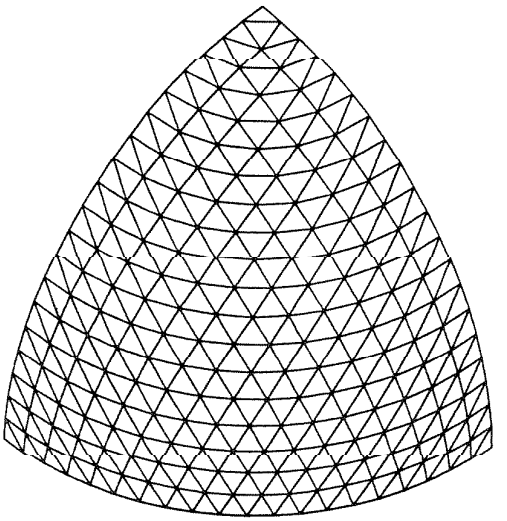

FIG. 2. Finite element model of one octant of spherical shell.

One octant of the shell was modeled with first-order triangular membrane/bending finite elements, as shown in Fig. 2. With 20 elements along each edge of the domain, the model has 231 wet points and 1263 structural DOF. Three planes of symmetry were imposed.

The numerical model was run for 15 drive frequencies in the nondimensional frequency range $ka = 0.5$–$ka = 5.0$, where a is the shell radius. Several of the drive frequencies are near critical frequencies, the first 13 of which are located at $ka = \pi$, 4.49, 5.76, 2π, 6.99, 7.73, 8.18, 9.10, 9.36, 3π, 10.4, 10.5, and 10.9 (see Ref. 37). Table I compares the numerical calculations and the closed-form solution for surface pressures, surface velocities, and farfield radiated pressures. Since the fundamental critical frequency occurs at $ka = \pi$, the constraints due to additional interior points (sometimes referred to as Chief points) were applied for all $ka > 2.7$. Four Chief points were used for these calculations. The calculations agree very closely with the closed-form solution for all ka's.

B. Radiation from a sector-driven spherical shell

A more challenging problem, both analytically and numerically, is the spherical shell with a uniform pressure drive over a sector, as shown in Fig. 3. (Here, we use the term "analytic" to refer to a series solution that converges to the exact solution.) The particular problem solved has the internal pressure load applied over the polar angle $\gamma = 36$ deg.

This problem was solved with the same finite element

TABLE I. Comparison of numerical solution with closed-form solution for uniformly driven spherical shell.

ka	Surface pressure (Pa) computed	exact	% error	Surface velocity (m/s) computed	exact	% error	Pressure at 100 m (Pa) computed	exact	% error
	($\times 10^{-1}$)	($\times 10^{-1}$)		($\times 10^{-7}$)	($\times 10^{-7}$)		($\times 10^{-2}$)	($\times 10^{-2}$)	
0.5	0.302	0.303	0.3	0.445	0.444	0.2	0.151	0.151	0.0
1.0	1.02	1.02	0.0	0.948	0.947	0.1	0.508	0.510	0.4
1.5	1.91	1.92	0.5	1.51	1.51	0.0	0.944	0.958	1.5
2.0	2.92	2.92	0.0	2.14	2.14	0.0	1.48	1.46	1.4
2.5	4.04	4.03	0.2	2.84	2.85	0.4	2.04	2.02	1.0
2.8	4.80	4.76	0.8	3.28	3.32	1.2	2.42	2.38	1.7
3.0	5.28	5.28	0.0	3.66	3.65	0.3	2.63	2.64	0.4
3.1	5.55	5.54	0.2	3.83	3.82	0.3	2.76	2.77	0.4
3.14	5.66	5.65	0.2	3.90	3.89	0.3	2.81	2.82	0.4
3.2	5.82	5.81	0.2	4.00	4.00	0.0	2.89	2.91	0.7
3.3	6.10	6.09	0.2	4.18	4.17	0.2	3.05	3.04	0.3
3.5	6.66	6.64	0.3	4.54	4.53	0.2	3.31	3.32	0.3
4.0	8.06	8.04	0.2	5.46	5.44	0.4	4.01	4.02	0.2
4.5	9.29	9.26	0.3	6.24	6.23	0.2	4.62	4.63	0.2
5.0	10.0	10.0	0.0	6.72	6.70	0.3	5.04	5.01	0.6

model used in the previous example (Fig. 2). Thus, with two load cases, both problems can be solved together. However, with a one-octant model of the sphere, the numerical solution of this problem requires running both symmetric and antisymmetric parts of the problem, providing a good check on the ability to handle multiple symmetry cases.

The benchmark solution to which the numerical results are compared is a series solution that we developed[38] based on equations given by Junger and Feit.[39] The results of this comparison are shown in Table II for four different nondimensional drive frequencies ka, where a is the radius of the sphere. For each drive frequency ka, the normalized farfield pressure $|pr/p_0a|$ is listed for each colatitude angle θ, where p is the farfield pressure at distance r from the origin, and p_0 is the internally applied pressure. The farfield pressure pattern for one of these frequencies ($ka = 5$) is also shown in Fig. 4. The numerical solution agrees very well with the exact solution, even at $ka = 2$, which coincides with a resonance of the submerged shell.

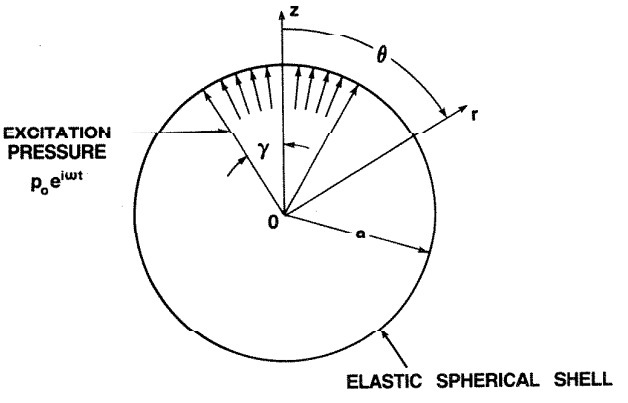

FIG. 3. Submerged elastic spherical shell driven over a sector.

C. Scattering from a spherical shell

Here, we demonstrate the ability to solve scattering problems by solving the problem of the submerged thin

TABLE II. Comparison of computed solution with converged series solution for sector-driven spherical shell.

ka	Colatitude θ (deg)	Normalized farfield pressure, $\lvert pr/p_0a\rvert$ computed	exact	% error
	0	0.0514	0.0514	0.0
	30	0.0445	0.0445	0.0
	60	0.0257	0.0258	0.4
0.5	90	0.0035	0.0035	0.0
	120	0.0258	0.0259	0.4
	150	0.0446	0.0446	0.0
	180	0.0515	0.0515	0.0
	0	0.0887	0.0889	0.2
	30	0.0744	0.0745	0.1
	60	0.0434	0.0434	0.0
1.0	90	0.0235	0.0237	0.8
	120	0.0448	0.0448	0.0
	150	0.0784	0.0786	0.3
	180	0.0939	0.0942	0.3
	0	1.183	1.163	1.7
	30	0.278	0.276	0.7
	60	0.667	0.666	0.2
2.0	90	0.131	0.128	2.3
	120	0.721	0.716	0.7
	150	0.757	0.695	8.9
	180	1.977	1.860	6.3
	0	0.507	0.512	1.0
	30	0.291	0.292	0.3
	60	0.020	0.017	17.6
5.0	90	0.096	0.097	1.0
	120	0.158	0.160	1.3
	150	0.164	0.163	0.6
	180	0.171	0.170	0.6

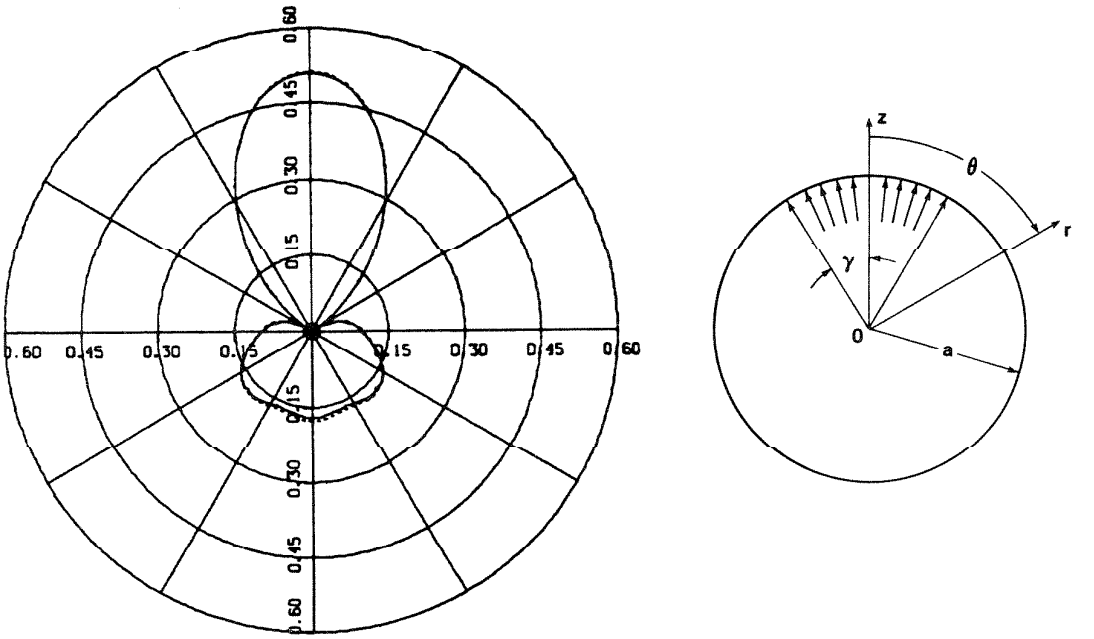

FIG. 4. Farfield radiated pressure $|pr/p_0a|$ at $ka = 5$ for a sector-driven spherical shell (solid line is exact; dashed line is computed).

spherical shell subjected to an incident time-harmonic planar wavetrain, as shown in Fig. 5. The solution of this problem exhibits rotational symmetry about the spherical axis parallel to the diretion of wave propagation. The benchmark solution to which the numerical results will be compared is the series solution published by Junger and Feit.[39]

The shell used is the same as in the two previous examples. Since the incident loading does not exhibit three planes of symmetry, the numerical solution of this problem requires decomposing the solution and the load into their symmetric and antisymmetric parts, thus providing a check on handling multiple symmetry cases for scattering problems.

The numerical model was run for several excitation frequencies in the nondimensional frequency range $ka < 20$, where a is the shell radius. Figure 6 shows a low-frequency comparison between the finite element calculation and the series solution for the farfield scattered pressure in the forward direction ($\theta = 180$ deg). The ordinate of this figure is the normalized pressure $|pr/p_0a|$, where p is the farfield scattered pressure at distance r from the origin and p_0 is the magnitude of the incident pressure. Again, the computed solution agrees very well with the exact (i.e., converged series) solution.

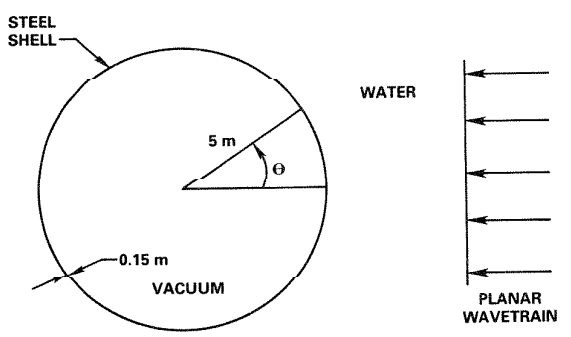

FIG. 5. Plane-wave scattering from an elastic spherical shell.

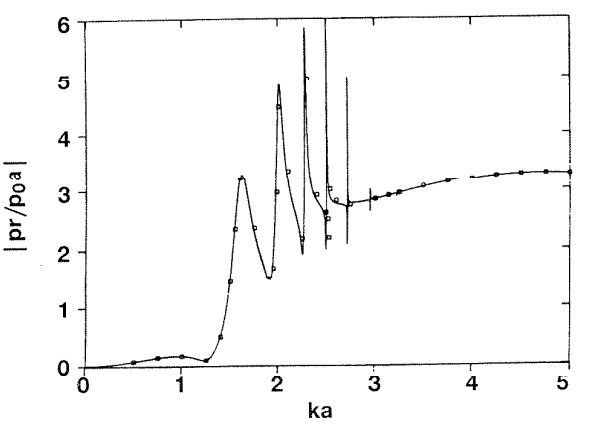

FIG. 6. Normalized farfield pressure $|pr/p_0a|$ scattered in the forward direction ($\theta = 180$ deg) by a spherical shell; solid curve is the converged series solution and square boxes are the numerical solution.

TABLE III. Comparison of computed solution with converged series solution for scattering from spherical shell; $\theta = 0$ corresponds to the backscattered direction.

ka	Angle θ (deg)	Normalized farfield pressure, $\lvert pr/p_0a \rvert$ computed	exact	% error
	0	0.0083	0.0081	2.5
	30	0.0144	0.0143	0.7
	60	0.0299	0.0299	0.0
0.5	90	0.0481	0.0481	0.0
	120	0.0626	0.0626	0.0
	150	0.0708	0.0708	0.0
	180	0.0734	0.0733	0.1
	0	0.0892	0.0903	1.2
	30	0.0382	0.0389	1.8
	60	0.0886	0.0886	0.0
1.0	90	0.1926	0.1930	0.2
	120	0.2208	0.2210	0.1
	150	0.1893	0.1887	0.3
	180	0.1662	0.1652	0.6
	0	3.146	3.149	0.1
	30	1.993	1.995	0.1
	60	0.325	0.320	1.6
1.6	90	1.515	1.498	1.1
	120	0.561	0.540	3.9
	150	2.058	2.092	1.6
	180	3.213	3.245	1.0
	0	0.155	0.160	3.1
	30	0.100	0.101	1.0
	60	0.067	0.069	2.9
4.0	90	0.268	0.269	0.4
	120	0.555	0.554	0.2
	150	1.757	1.757	0.0
	180	3.208	3.205	0.1

For several of the excitation frequencies, we also tabulate in Table III the farfield scattered pressure patterns. Again, agreement between the calculations and the series solution is excellent, even at $ka = 1.6$, which is near a resonant peak. At the sharper resonant peaks, the results would be much more sensitive to small changes in frequency.

This scattering problem was run again for ka's up to 20 to demonstrate the ability to compute in a frequency regime that includes numerous characteristic frequencies. Figure 7 shows comparisons of the numerical solution with the Junger–Feit series solution for both forward and backward scattering. The numerical calculation has converged even for the backscattered response, whose levels at many frequencies are significantly lower than in the forward direction. The numerical solution (which is almost indistinguishable from the series solution) was computed using the axisymmetric version of the program with 90 low-order, conical shell finite elements between the two spherical poles. Sixteen Chief points were placed along the spherical axis, and a frequency increment of $ka = 0.1$ was used. A structural loss factor of 0.01 was also used for this calculation.

III. COMPUTATIONAL ASPECTS

The numerical procedure outlined above is computationally intensive and could require many hours of supercomputer time for large problems. The principal problem-dependent parameters on which the computer time and memory depend are the number of independent structural DOF [denoted as "s" in the discussion following Eq. (1)], the number f of fluid DOF (the number of wet points on the fluid–structure interface), and the average wave front W_{avg} of the structural stiffness matrix. A related parameter is the root-mean-square matrix wave front W_{rms}, which is slightly larger than W_{avg} but will be used interchangeably with W_{avg} to simplify this discussion.

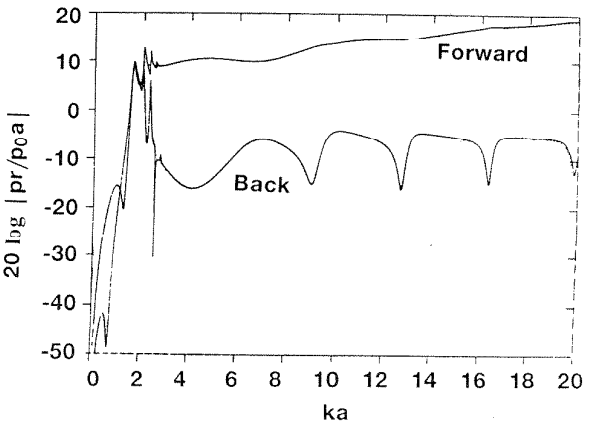

FIG. 7. Normalized farfield pressure 20 $\log\lvert pr/p_0a \rvert$ scattered in the forward and backward directions by a spherical shell; solid curves are for the converged series solution and dotted curves are for the numerical solution.

Three steps in the procedure have the potential to require large amounts of computer time: (1) the triangular factorization of H in Eq. (19), which requires $f^3/3$ complex operations (since H is fully populated, complex, and nonsymmetric); (2) the triangular factorization of Z (which is performed only once) in Eqs. (20)–(22), which requires $sW_{rms}^2/2$ complex operations, and (3) the forward/backward substitution (FBS) required in Eq. (20), in which the matrix $Z^{-1}GA$ is computed given the triangular factors of Z and the matrix product GA. This FBS requires $2sfW_{avg}$ complex operations. [Although the cost of FBS operations is usually insignificant in equation solving, this FBS step is significant because of the large number (f) of columns of GA.]

We note that the operation counts cited above are useful only as a general indication of the relative computer time required since, on a supercomputer, all these steps would be vectorized to the extent possible.

Although asymptotically (i.e., for very large problems) the factorization of H might be the most time-consuming operation, in practice the presence of internal structure increases the order s and wave front W_{avg} of the structural matrices, so that the FBS operation cited often requires the most time. To illustrate this point, we list in Table IV the statistics for several problems (not those presented in the preceding section).

TABLE IV. Number of complex operations for four problems.

Prob.	No. of structural DOF (s)	No. of fluid DOF (f)	Average wave front (W_{av})	Decomp. of H ($f^3/3$)	Decomp. of Z ($\simeq sW_{av}^2/2$)	FBS $Z^{-1}GA$ ($2sfW_{av}$)
1	2973	496	129	4.1×10^7	2.5×10^7	3.8×10^8
2	12 980	971	317	3.1×10^8	6.5×10^8	8.0×10^9
3	16 158	971	411	3.1×10^8	1.4×10^9	1.3×10^{10}
4	10 354	1786	138	1.9×10^9	9.9×10^7	5.1×10^9

IV. DISCUSSION

A very general computational capability has been described for predicting the acoustic sound-pressure field radiated or scattered by arbitrary three-dimensional elastic structures subjected to time-harmonic loads. Sufficient automation is provided so that, for many structures of practical interest, an existing finite element structural model can be adapted for acoustic analysis within a few hours.

One of the major benefits of having the acoustic analysis built around a general-purpose, finite element program is the ability to integrate the acoustic analysis of a structure with other dynamic and stability analyses. Thus the same finite element model can be used for modal analysis, frequency response analysis, linear shock analysis, and underwater acoustic analysis. In addition, many of the pre- and post-processors developed for use with the finite element package become available for acoustics as well.

[1]G. C. Everstine, "A Symmetric Potential Formulation for Fluid–Structure Interaction," J. Sound Vib. **79**, 157–160 (1981).

[2]G. C. Everstine, "Structural–Acoustic Finite Element Analysis, with Application to Scattering," in *Proceedings of the 6th Invitational Symposium on the Unification of Finite Elements, Finite Differences, and Calculus of Variations*, edited by H. Kardestuncer (Univ. of Connecticut, Storrs, CT, 1982), pp. 101–122.

[3]A. J. Kalinowski and C. W. Nebelung, "Media–Structure Interaction Computations Employing Frequency-Dependent Mesh Sizes with the Finite Element Method," Shock Vib. Bull. **51** (1), 173–193 (1981).

[4]L. H. Chen and D. G. Schweikert, "Sound Radiation from an Arbitrary Body," J. Acoust. Soc. Am. **35**, 1626–1632 (1963).

[5]F. M. Henderson, "A Structure–Fluid Interaction Capability for the NASA Structural Analysis (NASTRAN) Computer Program," Rep. 3962, David Taylor Naval Ship Research and Development Center, Bethesda, MD (1972).

[6]J. J. Engblom and R. D. Nelson, "Consistent Formulation of Sound Radiation from Arbitrary Structure," J. Appl. Mech. **42**, 295–300 (1975).

[7]D. T. Wilton, "Acoustic Radiation and Scattering From Elastic Structures," Int. J. Num. Meth. Eng. **13**, 123–138 (1978).

[8]I. S. Patel, "Radiation and Scattering from an Arbitrary Elastic Structure Using Consistent Fluid Structure Formulation," Comput. Struct. **9**, 287–291 (1978).

[9]J. S. Patel, "Analysis of Scattering and Radiation of Acoustic Waves from an Axisymmetric Structure in an Infinite Fluid Medium," Tech. Rep. 5821, Naval Underwater Systems Center, New London, CT (1980).

[10]I. C. Mathews, "A Symmetric Boundary Integral–Finite Element Approach for 3-D Fluid Structure Interaction," in *Advances in Fluid–Structure Interaction—1984*, edited by G. C. Everstine and M. K. Au-Yang (American Society of Mechanical Engineers, New York, 1984), PVP—Vol. 78 and AMD—Vol. 64, pp. 39–48.

[11]I. C. Mathews, "Numerical Techniques for Three-Dimensional Steady-State Fluid–Structure Interaction," J. Acoust. Soc. Am. **79**, 1317–1325 (1986).

[12]G. C. Everstine, F. M. Henderson, E. A. Schroeder, and R. R. Lipman, "A General Low Frequency Acoustic Radiation Capability for NASTRAN," in *Fourteenth NASTRAN Users' Colloquium* (National Aeronautics and Space Administration, Washington, DC, 1986), NASA CP-2419, pp. 293–310.

[13]G. C. Everstine, F. M. Henderson, and L. S. Schuetz, "Coupled NASTRAN/Boundary Element Formulation for Acoustic Scattering," in *Fifteenth NASTRAN Users' Colloquium* (National Aeronautics and Space Administration, Washington, DC, 1987), NASA CP-2481, pp. 250–265.

[14]G. C. Everstine, "Treatment of Static Preload Effects in Acoustic Radiation and Scattering," in *Sixteenth NASTRAN Users' Colloquium* (National Aeronautics and Space Administration, Washington, DC, 1988), NASA CP-2505, pp. 138–152.

[15]J. T. Hunt, M. R. Knittel, and D. Barach, "Finite Element Approach to Acoustic Radiation for Elastic Structures," J. Acoust. Soc. Am. **55**, 269–280 (1974).

[16]J. T. Hunt, M. R. Knittel, C. S. Nichols, and D. Barach, "Finite-Element Approach to Acoustic Scattering from Elastic Structures," J. Acoust. Soc. Am. **57**, 287–299 (1975).

[17]M. F. Werby and L. H. Green, "An Extended Unitary Approach for Acoustical Scattering from Elastic Shells Immersed in a Fluid," J. Acoust. Soc. Am. **74**, 625–630 (1983).

[18]M. F. Werby and G. J. Tango, "Application of the Extended Boundary Condition Equations to Scattering from Fluid-Loaded Objects," Eng. Anal. **5**, 12–20 (1988).

[19]P. Goswami, F. J. Rizzo, and D. J. Shippy, "Acoustic Scattering by Elastic Solids Using the Boundary Element Method," Rev. Quantitative Nondestruct. Eval. **7**, 95–102 (1987).

[20]L. H. Chen, "Acoustic Emissions from Submerged Structures," in *Developments in Boundary Element Methods—2*, edited by P. K. Banerjee and R. P. Shaw (Applied Science, London, 1982), Chap. 9, pp. 245–281.

[21]"NASTRAN User's Manual," NASA SP-222 (08) [Computer Software Management and Information Center (COSMIC), University of Georgia, Athens, GA, 1986].

[22]"MSC/NASTRAN User's Manual," The MacNeal–Schwendler Corporation, Los Angeles, CA (1985).

[23]G. C. Everstine, "Structural Analogies for Scalar Field Problems," Int. J. Num. Meth. Eng. **17**, 471–476 (1981).

[24]G. C. Everstine, "Dynamic Analysis of Fluid-Filled Piping Systems Using Finite Element Techniques," ASME Trans. J. Press. Vessel Tech. **108**, 57–61 (1986).

[25]R. R. Lipman, "Computer Animation of Modal and Transient Vibrations," in *Fifteenth NASTRAN Users' Colloquium* (National Aeronautics and Space Administration, Washington, DC, 1987), NASA CP-2481, pp. 88–97.

[26]G. Chertock, "Integral Equation Methods in Sound Radiation and Scattering from Arbitrary Surfaces," Rep. 3538, David Taylor Naval Ship Research and Development Center, Bethesda, MD (1971).

[27]E. A. Schroeder, "A New Block Solver for Large, Full, Unsymmetric, Complex Systems of Linear Algebraic Equations," Rep. 88/003, David Taylor Research Center, Bethesda, MD (1988).

[28]H. Lamb, *Hydrodynamics* (Dover, New York, 1945), 6th ed.
[29]H. A. Schenck, "Improved Integral Formulation for Acoustic Radiation Problems," J. Acoust. Soc. Am. **44**, 41–58 (1968).
[30]A. J. Burton and G. F. Miller, "The Application of Integral Equation Methods to the Numerical Solution of Some Exterior Boundary-Value Problems," Proc. R. Soc. London Series A **323**, 201–210 (1971).
[31]F. J. Rizzo, D. J. Shippy, and M. Rezayat, "Boundary Integral Equation Analysis for a Class of Earth–Structure Interaction Problems," Final National Science Foundation Project Report, University of Kentucky, Lexington, KY (1985).
[32]M. Rezayat, D. J. Shippy, and F. J. Rizzo, "On Time-Harmonic Elastic-Wave Analysis by the Boundary Element Method for Moderate to High Frequencies," Comp. Meth. Appl. Mech. Eng. **55**, 349–367 (1986).
[33]C. T. M. Chang, "Natural Resonant Frequency of a Prolate Acoustical Resonator," J. Acoust. Soc. Am. **49**, 611–614 (1971).
[34]W. C. Ghering, *Reference Data for Acoustic Noise Control* (Ann Arbor Science, Ann Arbor, MI, 1978).
[35]L. E. Kinsler, A. R. Frey, A. B. Coppens, and J. V. Sanders, *Fundamentals of Acoustics* (Wiley, New York, 1982), 3rd ed.
[36]H. Huang and Y. F. Wang, "Asymptotic Fluid–Structure Interaction Theories for Acoustic Radiation Prediction," J. Acoust. Soc. Am. **77**, 1389–1394 (1985).
[37]H. Huang, "Helmholtz Integral Equations for Fluid–Structure Interaction," in *Advances in Fluid–Structure Interaction—1984*, edited by G. C. Everstine and M. K. Au-Yang (American Society of Mechanical Engineers, New York, 1984), PVP—Vol. 78 and AMD—Vol. 64, pp. 19–38.
[38]F. M. Henderson, "RADSPHERE—A Computer Program for Calculating the Steady-State, Axially Symmetric, Forced Response and Radiation Field of a Submerged Spherical Shell," Rep. 87/031, David Taylor Naval Ship Research and Development Center, Bethesda, MD (1987).
[39]M. C. Junger and D. Feit, *Sound, Structures, and Their Interaction* (MIT, Cambridge, MA, 1986), 2nd ed.